Article

Developmental Cell

# The Triple-Repeat Protein Anakonda Controls Epithelial Tricellular Junction Formation in *Drosophila*

## Highlights

- Bicellular and tricellular occluding junctions form independently in *Drosophila*
- The transmembrane protein Anakonda localizes to epithelial tricellular junctions
- Anakonda is crucial for epithelial barrier function and tricellular junction assembly
- Anakonda promotes the accumulation of Gliotactin at tricellular junctions

## Authors

Sunitha Byri, Tvisha Misra, ..., Anne Uv, Stefan Luschnig

## Correspondence

anne.uv@gu.se (A.U.), luschnig@uni-muenster.de (S.L.)

## In Brief

Tricellular junctions (TCJs) facilitate three-way contacts among cells and mediate barrier function. Only few TCJ components have been described. Byri et al. show that Anakonda, a transmembrane protein with unusual triple-repeat structure, localizes to TCJs and is essential for organizing their assembly at cell corners independently of bicellular junction formation.

Byri et al., 2015, Developmental Cell *33*, 535–548
June 8, 2015 
http://dx.doi.org/10.1016/j.devcel.2015.03.023

CellPress

Developmental Cell
Article

# The Triple-Repeat Protein Anakonda Controls Epithelial Tricellular Junction Formation in *Drosophila*

Sunitha Byri,[1,6] Tvisha Misra,[5,6] Zulfeqhar A. Syed,[1] Tilmann Bätz,[5] Jimit Shah,[5] Lukas Boril,[5] Jade Glashauser,[5] Tinri Aegerter-Wilmsen,[5] Till Matzat,[3,4] Bernard Moussian,[2] Anne Uv,[1,*] and Stefan Luschnig[3,4,5,*]
[1]Institute of Biomedicine, University of Gothenburg, Medicinaregatan 9A, 40530 Gothenburg, Sweden
[2]Interfaculty Institute for Cell Biology, University of Tübingen, Auf der Morgenstelle 15, 72076 Tübingen, Germany
[3]Institute of Neurobiology, University of Münster, Badestrasse 9, 48149 Münster, Germany
[4]Cluster of Excellence EXC 1003, Cells in Motion, CiM, 48149 Münster, Germany
[5]Institute of Molecular Life Sciences, University of Zürich, Winterthurerstrasse 190, 8057 Zürich, Switzerland
[6]Co-first author
*Correspondence: anne.uv@gu.se (A.U.), luschnig@uni-muenster.de (S.L.)
http://dx.doi.org/10.1016/j.devcel.2015.03.023

## SUMMARY

**In epithelia, specialized tricellular junctions (TCJs) mediate cell contacts at three-cell vertices. TCJs are fundamental to epithelial biology and disease, but only a few TCJ components are known, and how they assemble at tricellular vertices is not understood. Here we describe a transmembrane protein, Anakonda (Aka), which localizes to TCJs and is essential for the formation of tricellular, but not bicellular, junctions in *Drosophila*. Loss of Aka causes epithelial barrier defects associated with irregular TCJ structure and geometry, suggesting that Aka organizes cell corners. Aka is necessary and sufficient for accumulation of Gliotactin at TCJs, suggesting that Aka initiates TCJ assembly by recruiting other proteins to tricellular vertices. Aka's extracellular domain has an unusual tripartite repeat structure that may mediate self-assembly, directed by the geometry of tricellular vertices. Conversely, Aka's cytoplasmic tail is dispensable for TCJ localization. Thus, extracellular interactions, rather than TCJ-directed intracellular transport, appear to mediate TCJ assembly.**

## INTRODUCTION

Epithelial cells are linked via intercellular junctions that provide paracellular diffusion barriers, maintenance of polarity, and cell-to-cell communication. Bicellular junctions (BCJs) make up the most abundant intercellular contacts in epithelia. They connect two neighboring plasma membranes and are organized into distinct complexes along the apical-basal axis, collectively forming the apical junctional belt. However, at certain positions along the cell perimeter, three cell corners meet and the bicellular junctional complex is disjointed. Here, specialized tricellular junctions (TCJs) connect epithelial cells (Staehelin, 1973; Fristrom, 1982; Graf et al., 1982; Noirot-Timothée et al., 1982). TCJs play important roles in epithelial barrier functions (Ikenouchi et al., 2005; Riazuddin et al., 2006; Krug et al., 2009; Furuse et al., 2014) and cytoskeletal organization (Oda et al., 2014), and are preferential sites for trans-endothelial migration of neutrophils (Burns et al., 1997) and metastatic cancer cells (Nakai et al., 2005), as well as for the spreading of intracellular pathogens (Fukumatsu et al., 2012).

Due to the geometry of three-cell vertices, the sealing of the epithelium at these sites requires a dedicated junctional organization. Ultrastructural analyses using freeze-fracture electron microscopy (EM) showed that the zonula occludens, tight junctions (TJs) in vertebrates and septate junctions (SJs) in arthropods (Furuse and Tsukita, 2006; Banerjee et al., 2008), changes characteristics when approaching a three-cell vertex. Instead of continuing parallel to the epithelial plane around the cell perimeter, the junctional strands extend basally, forming a bicellular seal along the apical-basal axis (Staehelin, 1973). In vertebrates, these structures are termed central sealing elements, and three such parallel TJ extensions enclose a narrow (approximately 10 nm) central canal at each TCJ (Staehelin, 1973). Similarly, in invertebrates the SJ strands turn by 90 degrees when approaching a tricellular corner, forming three parallel limiting strands that surround the tricellular juncture space, resembling the central sealing element in vertebrates (Noirot-Timothee and Noirot, 1980; Fristrom, 1982; Graf et al., 1982; Noirot-Timothée et al., 1982). Within and perpendicular to the vertical juncture space are a series of diaphragms, which appear linked not only to three limiting septa, but also to the three cell corner membranes, thereby forming true tricellular contacts (Fristrom, 1982; Graf et al., 1982; Noirot-Timothée et al., 1982).

Despite the fundamental biological importance of TCJs, only few of their components are known (Furuse et al., 2014), and the mechanism of their localized assembly at three-cell vertices is not understood. In vertebrates, the Occludin family protein Tricellulin localizes to TCJs (Ikenouchi et al., 2005) and is recruited there by lipolysis-stimulated lipoprotein receptor (LSR) and related proteins (ILDR1 and ILDR2; Masuda et al., 2011; Higashi et al., 2013). Additionally, the cytoplasmic PDZ-domain-containing protein Tjp2iso3 associates with Tricellulin in Sertoli cells

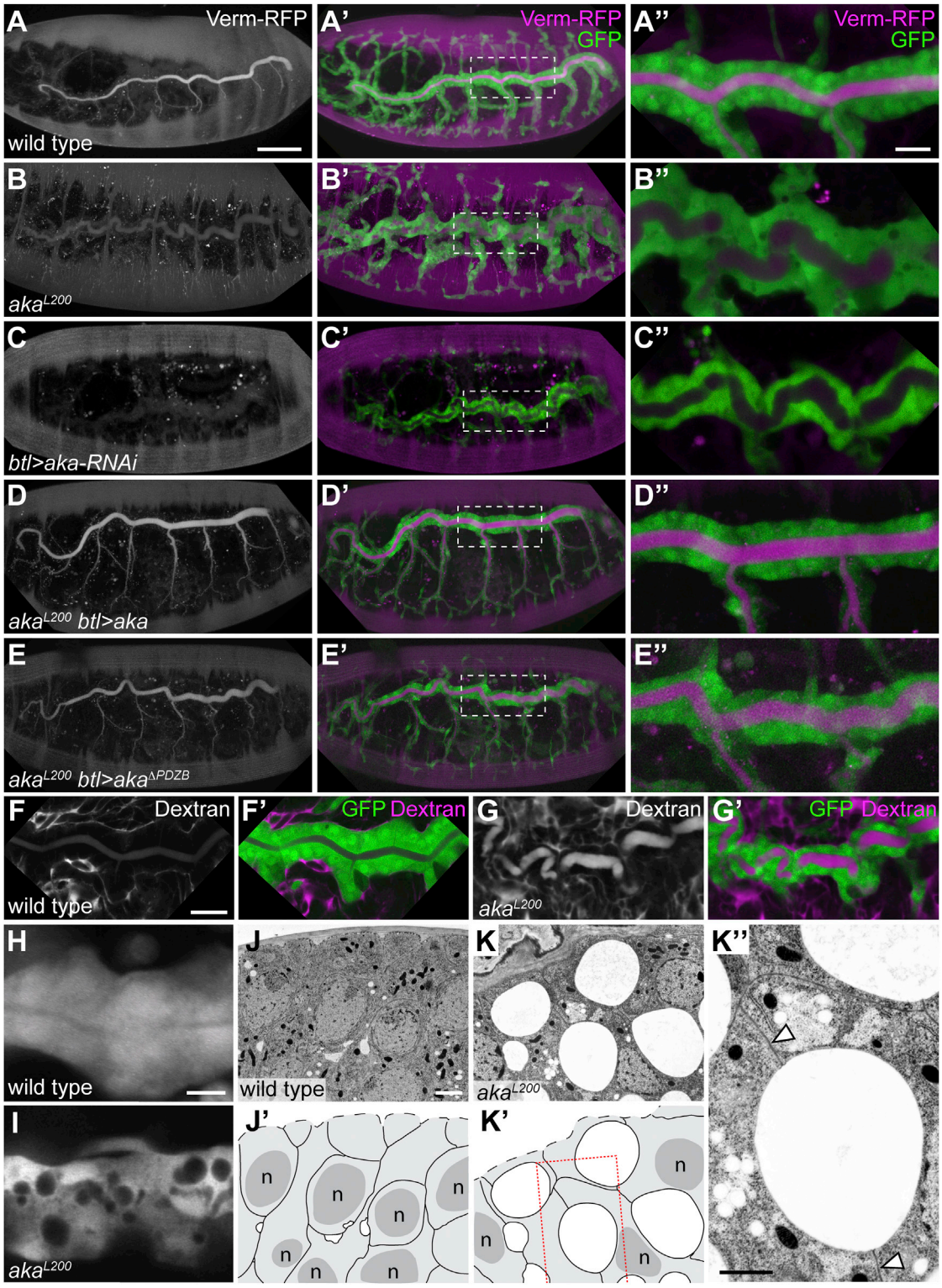


**Figure 1. *aka* Is Required for Tracheal Tube Size Control and Epithelial Barrier Formation**

(A–E) Living stage 16 embryos expressing cytoplasmic GFP (green) and secreted Verm-RFP (magenta) in tracheal cells. *aka* mutants (B) and embryos expressing *UAS-aka*$^{RNAi}$ in tracheal cells under the control of *btl*-Gal4 (C) show over-elongated tracheal tubes with reduced levels of luminal Verm-RFP, compared to the wild-type (A). The tracheal defects of *aka* embryos are rescued by tracheal specific expression of wild-type Aka (*UAS-aka*, D) or of an Aka variant lacking the C-terminal PDZ-binding motif (*UAS-akaΔPDZB*, E). Right-hand images (A′′–E′′) show close-up views of boxed regions in (A′–E′).

*(legend continued on next page)*

(Chakraborty et al., 2014). The Neuroligin-like transmembrane protein Gliotactin in *Drosophila* is the only TCJ protein characterized so far in invertebrates (Schulte et al., 2003). It is not clear what kind of cues direct the accumulation of these proteins at tricellular vertices, and the features of known TCJ proteins do not explain the distinct structure of three-cell contacts observed by EM. Here, we describe a transmembrane protein, Anakonda (Aka), which accumulates at TCJs in *Drosophila* epithelia. Aka can initiate TCJ assembly and may do so through its large extracellular domain, which exhibits an unusual triple-repeat structure.

## RESULTS

### *anakonda* Mutants Develop Over-elongated Tracheae and Epithelial Barrier Defects

In a mutagenesis screen, we isolated an embryonic lethal complementation group with nine alleles that showed excessively elongated tracheal tubes (Figures 1A and 1B). We named the locus *anakonda* (*aka*) based on the tortuous tube phenotype. In addition, *aka* mutants showed reduced levels of the secreted protein Vermiform-RFP (Verm-RFP; Förster et al., 2010) in the tracheal lumen (Figures 1A and 1B). These phenotypes are characteristic for mutants lacking epithelial barrier function due to mutations in SJ components (Behr et al., 2003; Paul et al., 2003; Wu et al., 2004). To assess epithelial barrier function, we injected Rhodamine-labeled dextran (10 kDa) into the hemocoel of stage 16 *aka* and control embryos, and followed the distribution of fluorescent signals. While dextran was largely excluded from lumina of hindgut, salivary glands, and tracheae in wild-type embryos (Figure 1F), dextran was readily detectable in the lumina of these organs in *aka* embryos 20 min after injection (Figure 1G), indicating that epithelial barrier function was defective.

Besides these defects, stage 17 *aka* embryos showed "cavities" in the tracheal epithelium, seen as round areas, 0.5–6 μm in diameter, from which cytoplasmic GFP was excluded (Figures 1H and 1I). Similar structures were evident in the epidermis of *aka* embryos. EM analyses revealed that the cavities are lined by two lateral plasma membranes, indicating that they form between neighboring cells (Figures 1J and 1K), reminiscent of delaminations previously observed in embryos that lack the TCJ protein Gli (Schulte et al., 2003). Because SJs were observed on either side of the paracellular cavities, they appear to be associated with focal loss of cell-cell adhesion.

### *anakonda* Encodes a Large Transmembrane Protein with a Tripartite Extracellular Domain

We mapped the *aka* locus and identified a lethal PBac insertion (*PBac*$^{YD1046}$; Quiñones-Coello et al., 2007) in the *CG3921* gene that failed to complement *aka* alleles. Furthermore, tracheal-specific knockdown of *CG3921* by RNAi led to over-elongated tracheae and reduced luminal Verm-RFP levels, resembling the *aka* loss-of-function phenotype (Figure 1C; Jaspers et al., 2012), whereas tracheal-specific expression of a UAS-*aka* transgene rescued the tracheal defects of *aka* embryos (Figure 1D). We conclude that *aka* mutations affect the *CG3921* gene, which we refer to as *aka*.

Three annotated *aka* transcripts yield two protein isoforms of 3,115 and 3,123 amino acids (aa; Figure 2A), which share an N-terminal signal peptide, a large extracellular domain (2,674 or 2,682 aa), a transmembrane domain, and an intracellular domain (384 aa) with a class-I PDZ-binding motif (ETAM) at the C terminus (Figure 2B). Domain prediction using Simple Modular Architecture Research Tool (SMART; Schultz et al., 1998) indicated three Scavenger Receptor (SR) cysteine-rich domains, a complement/UEGF/BMP1 (CUB) domain, a C-type lectin domain, and 19 parallel beta-helix (PBH) motifs in the extracellular part. However, in sequence homology searches, parts of the extracellular domain self-aligned over three non-overlapping regions that extend beyond the three annotated SR domains. To explore if Aka might contain extended internal repeats, we retrieved multiple protein alignments of Aka homologs from fourteen species and used profile hidden Markov models (HMM; http://hmmer.janelia.org/) based on these alignments to search for similarities (Figure S1). We found that an 816 aa profile-HMM targets three successive regions of *D. melanogaster* Aka that we term regions I–III (Figure 2C). Whereas region I aligns to the entire profile-HMM, regions II and III each display a single central gap in the alignment of 248 and 289 aa, respectively. Protein structure predictions (Phyre; Kelley and Sternberg, 2009) suggested that region II and III both exhibit a CUB-like fold (confidence >90%), similar to the annotated CUB domain in the central part of region I. In addition, each of the three regions shares a predicted scavenger-receptor-like fold at the N terminus and a single-stranded right-handed beta-helix motif at the C terminus (Figure 2C). Together, these analyses predict three tandem repeat regions that together span approximately 2,500 of the 2,691 aa long extracellular domain. Strikingly, the pattern and spacing of the three repeats and the overall size of the extracellular domain are conserved between Aka homologs from diverse invertebrates and a cephalochordate, suggesting they are of functional importance (Figure S1). The cytoplasmic portion contains no conserved domains, but the C-terminal PDZ-binding motif is conserved among Aka homologs in insects and nematodes. Thus, Aka is a conserved transmembrane protein whose extracellular part comprises an unusual tripartite structure.

### *aka* Mutations Affect the Extracellular Part of Aka

We identified mutations in the *aka* coding region in seven EMS-induced *aka* alleles (Figures 2A and 2B). Three alleles carry

(F and G) Embryos expressing cytoplasmic GFP (green) in tracheal cells were injected with fluorescent 10 kDa dextran (magenta) at stage 16. Dextran is largely excluded from the tracheal lumen of wild-type embryos (F), but rapidly enters the lumen in *aka* mutants (G).

(H and I) Close-ups of tracheal transverse connective in living wild-type (H) and *aka* embryos (I) expressing cytoplasmic GFP. Note the cavities devoid of GFP in the *aka*-mutant epithelium.

(J–K″) TEM sections of wild-type (J) and *aka* mutant (K) epidermis with schematic drawings (J′ and K′) to indicate plasma membranes and nuclei ("n"). Each cavity in (K) is flanked by two BCJs, indicating that cavities form between two cells. (K″) Higher magnification of the region marked by a box in (K′). Arrowheads point to two BCJs flanking a cavity.

Scale bars represent 50 μm (A–E), 10 μm (A″–E″), 20 μm (F and G), 5 μm (H and I), 2 μm (J and K), and 2 μm (K″).

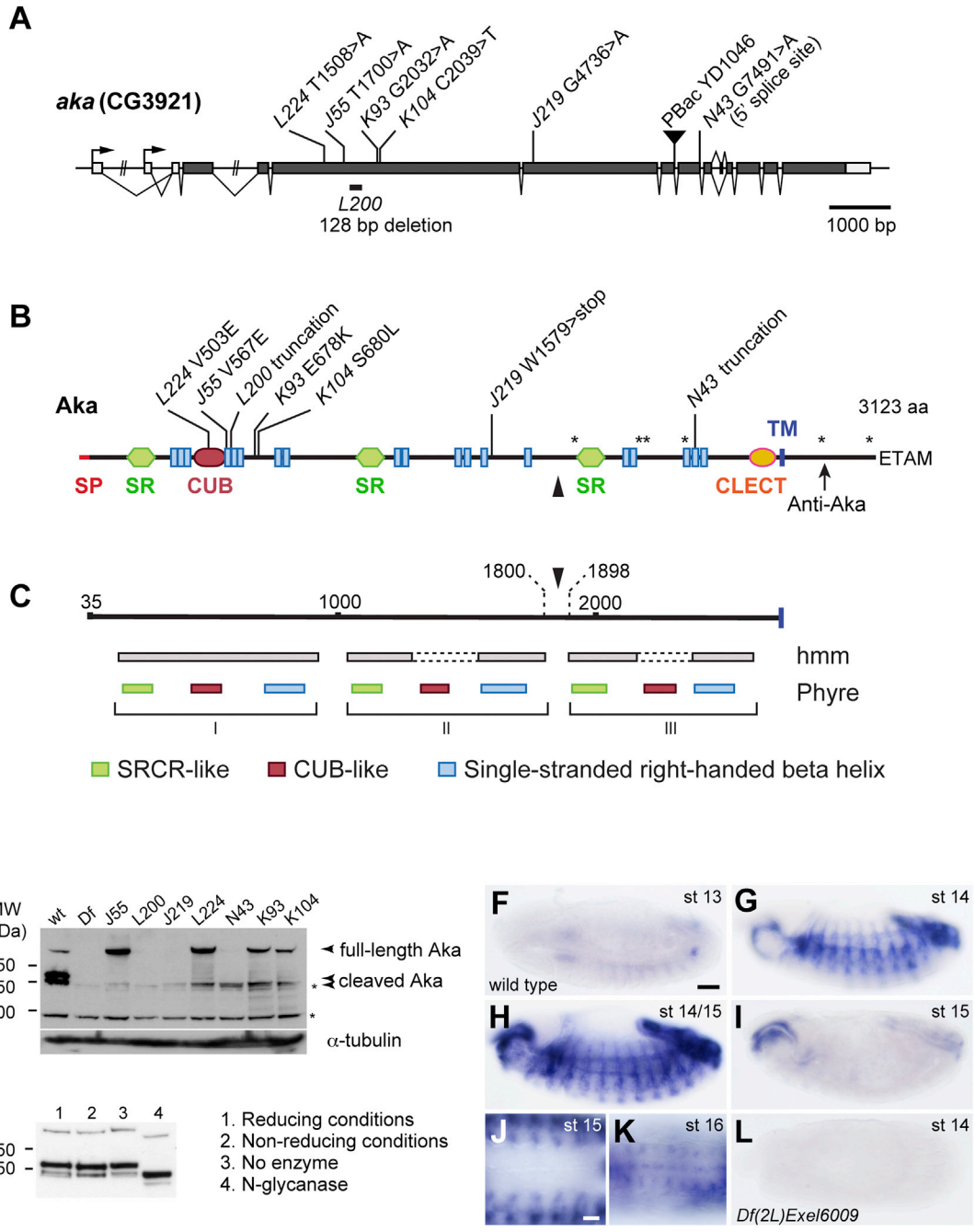


**Figure 2. *aka* Encodes a Large Transmembrane Protein with a Tripartite Extracellular Domain**

(A) Genomic organization of the *aka* locus. Exons are shown as boxes with coding regions in black.

(B) Domain organization of Aka protein. The signal peptide (SP), extracellular domain (2716 aa), transmembrane domain (TM), and cytoplasmic tail (384 aa) with the PDZ-binding motif (ETAM) are indicated. SMART predicts three scavenger receptor cysteine-rich domains (SR), a CUB domain, a C-type lectin domain (CLECT), and nineteen parallel beta-helix repeats (blue) in the extracellular part. Mutations in *aka* alleles are indicated. The anti-Aka antiserum was raised against a peptide in the cytoplasmic part (arrow). Asterisks indicate the positions of the six tryptic peptides detected for the C-terminal Aka cleavage product.

(C) Aka's extracellular domain exhibits a tripartite repeat structure. Phyre predicts an N-terminal SR domain, a central CUB-like domain and a C-terminal single-stranded right-handed beta helix in each repeat (colored boxes; 84%–100% confidence). Hmmer indicates similarity in the N- and C-terminal regions between each repeat. Grey boxes show regions that align with the 816 aa profile-hmm. Conditional E values are 0.0 for region I, $7.0 \times 10^{-34}$ and $1.9 \times 10^{-8}$ for region II, and $1.0 \times 10^{-37}$ and $9.5 \times 10^{-4}$ for region III. Arrowhead indicates the approximate Aka cleavage site.

(D and E) Immunoblot of embryonic extracts probed with anti-Aka. (D) Wild-type embryos produce full-length Aka above 250 kDa and two smaller Aka species around 150 kDa (arrowheads). Asterisks indicate non-specific bands also detected in *Df(2L)BSC171* ("Df") embryos. Specific Aka signals are absent from $aka^{L200}$, $aka^{N43}$ and $aka^{J210}$ embryos, whereas full-length Aka, but not the lower-MW species, are present in *aka* mis-sense alleles ($aka^{J55}$, $aka^{L224}$, $aka^{K93}$, $aka^{K104}$).

*(legend continued on next page)*

mutations that cause C-terminal truncations in the extracellular part. $aka^{L200}$ contains a 128-bp deletion in the third coding exon, resulting in a frame shift and a premature stop codon six codons thereafter. The predicted protein product (587 aa) is truncated after the CUB domain in region I. $aka^{N43}$ contains a G to A transition in the 5′ splice site of intron 9. Retention of the intron and translation of the mutant mRNA results in a premature stop codon in region III, yielding a predicted truncated protein of 2,394 aa. $aka^{J219}$ contains a premature stop codon (W1579*) in region II. Four *aka* alleles contain missense mutations in the extracellular part, each leading to a single amino acid exchange in region I ($aka^{K93}$, E678K; $aka^{J55}$, V567E; $aka^{K104}$, S680L; $aka^{L224}$, V503E). Thus, all of the identified EMS-induced *aka* mutations affect the extracellular part of the protein.

We raised antisera against a peptide located in the cytoplasmic domain (Figure 2B). On immunoblots, a band well above 250 kDa was detected in extracts from wild-type embryos, but not from *Df(2L)BSC171* homozygotes, suggesting that this band represents full-length Aka protein (predicted molecular weight (MW) 350 kDa; Figure 2D). Two additional bands of lower MW (around 150 kDa) may represent proteolytic cleavage products. Electrophoretic mobility of the three Aka species was the same under reducing and non-reducing conditions (Figure 2E), indicating that they are not linked by disulphide bridges. However, treatment of extracts with N-glycanase caused a mobility shift of all three species, suggesting that they are N-glycosylated (Figure 2E). The MW of the smaller species (below 150 kDa) suggests cleavage beyond residue 1,800. Trypsin digestion and peptide identification by LC-MS/MS of the smaller species yielded six peptides that cover amino acids 1,898–3,085, arguing that cleavage occurs between extracellular repeats II and III (between residues 1,800–1,898; Figures 2B and 2C). In *aka* mutants predicted to produce C-terminally truncated proteins ($aka^{L200}$, $aka^{N43}$, $aka^{J219}$), none of the three specific bands was detectable, whereas the four *aka* alleles with missense mutations in repeat I ($aka^{J55}$, $aka^{L224}$, $aka^{K93}$, $aka^{K104}$) produced full-length Aka and little if any cleavage products (Figure 2D). Because full-length Aka in *aka* missense mutants showed similar mobility as in wild-type embryos, these mutations appear not to prevent initial steps of N-glycosylation, but preclude the apparent proteolytic processing of Aka.

## Aka Accumulates at Epithelial Tricellular Junctions

In situ hybridization revealed *aka* expression in ectodermal epithelia (epidermis, foregut, hindgut, salivary glands, tracheae; Figures 2F–2H and 2L) from stage 13. Expression in epithelia declined from late stage 15 (Figure 2I) and *aka* transcripts appeared in the CNS during stage 16 (Figures 2J and 2K). This expression pattern resembles those of SJ components that participate in epithelial and blood-brain-barrier functions.

Consistent with transcript analyses, Aka protein was detectable by immunostaining in embryonic epithelia and CNS (Figure 3; Figure S2) of wild-type, but not $aka^{L200}$ embryos (Figures 3B and 3G). Moreover, a genomic Aka transgene carrying a Ty1-Tev-SGFP-FLAG tag in the cytoplasmic domain showed the same distribution as endogenous Aka protein and rescued *aka* mutants (Figures S2L–S2O). In sagittal sections of the epidermis, Aka was strongly enriched at junctions between three adjoining cells (Figure 3C). Aka was also detectable at BCJs, with on average 18-fold lower levels compared to TCJs (Figures S2A, S2B, and S2N). At TCJs, Aka overlapped with the SJ protein Discs Large (Dlg; Woods and Bryant, 1991) along the apicolateral membrane domain (Figures 3H and 3I), and localized just basally to adherens junctions marked by beta-Catenin/Armadillo (Arm; Figures 3E–3G). In embryos homozygous for *aka* missense mutations ($aka^{K104}$, $aka^{K93}$, $aka^{J55}$, $aka^{L224}$), Aka was distributed inside cells (Figure 3D and data not shown), suggesting that the mutant Aka proteins are retained intracellularly or are internalized from the plasma membrane.

We compared the distribution of Aka and Gli using a Gli-YFP protein trap or anti-Gli antisera. We found that Aka and Gli colocalize at TCJs, both in ectoderm-derived epithelia that exhibit pleated SJs (Figures 3K and 3L; Figures S2C–S2I) and in the endodermal midgut that develops smooth SJs involving a different set of SJ proteins (Figure 3J; Figure S2K; Izumi et al., 2012), as well as in the extra-embryonic amnioserosa (Figure S2J). The presence of Aka and Gli at TCJs in ectodermal and endodermal epithelia suggests that the two proteins are common components of TCJs.

## *aka* Is Required for the Formation of Tricellular, but Not Bicellular Junctions

Because the *aka* phenotype resembled mutants in SJ components, we asked whether SJ proteins were mislocalized in *aka* mutants. Fasciclin 3 (Fas3; Snow et al., 1989) concentrates at SJs without being required for viability (Whitlock, 1993), and becomes evenly distributed along lateral membranes in mutants with an impaired paracellular barrier (Behr et al., 2003; Paul et al., 2003; Wu et al., 2004). Fas3 was indeed mislocalized in epithelia of *aka* embryos (Figures 4A and 4B). In contrast, the claudin-like protein Sinuous (Sinu; Figures 4A and 4B; Wu et al., 2004), the Na pump $\alpha$-subunit (Atp$\alpha$; Figures 4C and 4D; Paul et al., 2003), and the ERM protein Coracle (Cora; Figures 4E and 4F; Lamb et al., 1998), all of which are SJ core complex components (Oshima and Fehon, 2011), remained concentrated at apico-lateral membranes in *aka* mutants. Similarly, apicolateral accumulation of the SJ-associated membrane proteins Lachesin (Lac)-YFP (Figures S3A and S3B; Llimargas et al., 2004) and Melanotransferrin (MTf; Tiklová et al., 2010; not shown) was not affected in *aka* mutants. The cytoplasmic polarity proteins Dlg, Scribble (Scrib; Bilder and Perrimon, 2000) and

(E) Incubation of extracts with N-glycanase causes a shift in Aka mobility (lanes 3 and 4), suggesting that Aka is N-glycosylated. Non-reducing conditions do not alter electrophoretic mobility (lanes 1 and 2).

(F–L) In situ hybridization shows *aka* expression in embryonic epithelia and CNS. Expression is first detected at stage 13 (F), increases in epidermis, tracheae, foregut, and hindgut during stages 14 and 15 (G and H), and declines at late stage 15 (I; lateral views, dorsal up). CNS expression is detectable from stage 16 (J and K, ventral views). No transcripts were detected in *Df(2L)Exel6009* embryos (L).

Scale bars represent 50 μm (F–I, L), and 10 μm (J and K).

See also Figure S1.

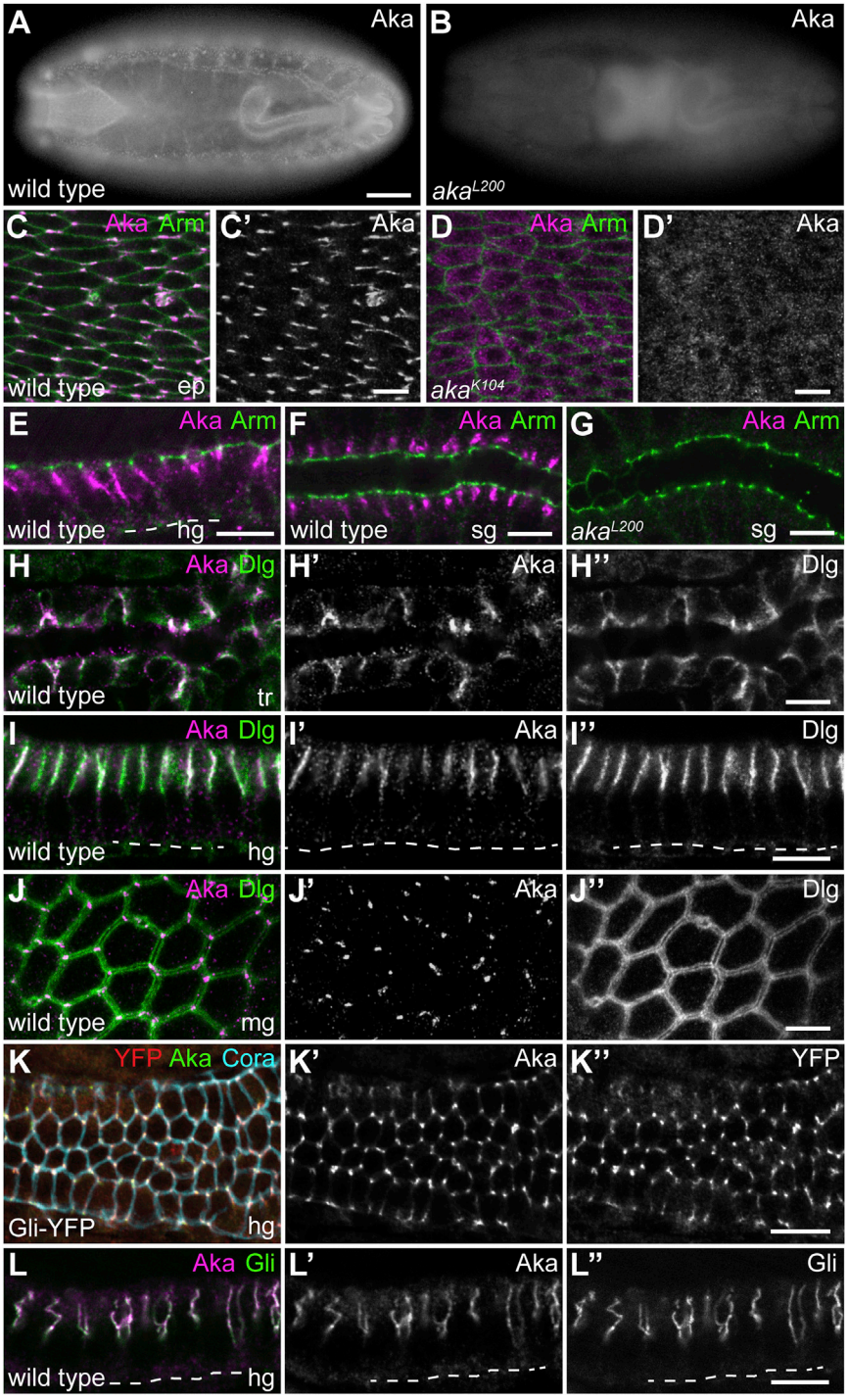


**Figure 3. Aka Protein Accumulates at Tricellular Junctions**

(A and B) Epifluorescence images of stage 16 embryos labeled with anti-Aka show Aka protein in the epidermis, tracheae, and hindgut in the wild-type (A), whereas only autofluorescent signals are seen in *aka*$^{L200}$ embryos (B).

(C–G) Confocal sections of stage 16 embryos co-labeled with anti-Aka (magenta) and anti-Arm (green). Aka localization at TCJs is shown by en face view of wild-type epidermis (ep; C and C′). In *aka*$^{K104}$ homozygotes, Aka is detected intracellularly (D and D′). Lateral views of hindgut (hg; E) and salivary gland (sg; F and G) epithelia reveal Aka localization just basal to adherens junctions labeled by Arm. No Aka staining is detected in *aka*$^{L200}$ homozygotes shown here for salivary glands (G).

(H and I) Cross-sections of tracheal (tr; H–H″) and hindgut (I–I″) epithelia of wild-type embryos labeled with anti-Aka (magenta) and anti-Dlg (green) show overlapping distribution of Aka and Dlg along the apical-basal axis. Stippled line in (I) indicates the basal cell surface.

(J) Aka is detected at TCJs in the endodermal midgut (mg) epithelium (J–J″; en face view, Z projection).

(K) En face view of hindgut epithelium of an embryo expressing Gli-YFP. Triple labeling for YFP (red), Aka (green), and Cora (blue) demonstrates co-localization of Aka and Gli at TCJs.

(L) Lateral view of hindgut epithelium in wild-type embryo labeled with anti-Aka (magenta) and anti-Gli (green) shows co-localization of the two proteins along the apical to basal axis of TCJs. Stippled line indicates the basal surface.

Scale bars represent 50 μm (A and B); all other images, 5 μm.

See also Figure S2.

Lethal giant larvae (Lgl; Mechler et al., 1985) also localize to SJs, but are more mobile than the core complex (Oshima and Fehon, 2011). Dlg, Scrib, and Lgl were concentrated apico-laterally in *aka* mutants, similar to wild-type controls (Figures 4G–4J and data not shown). All embryos were analyzed at early stage 16, when SJ components show apico-lateral localization and epithelia have developed functional paracellular barriers (Tepass and Hartenstein, 1994). The results therefore suggest that Aka is not required for assembly of bicellular SJs.

To address if recruitment of Aka to TCJs could depend on bicellular SJ formation, we analyzed Aka localization in *cora* embryos, in which SJs are severely reduced or absent (Lamb et al., 1998). Aka accumulated at TCJs in *cora* mutants with similar intensity as in controls, and retained its apico-lateral localization, unlike Fas3, which distributed along the entire lateral membrane (Figures 4K–4N). Aka also accumulated at TCJs in *Mcr*, *Nrg* and *sinu* mutants, which lack SJs (Figures S3C–S3F; Genova and Fehon, 2003; Wu et al., 2004; Bätz et al., 2014). Thus, Aka appears to localize to TCJs by a mechanism that is independent of bicellular SJ formation.

We next analyzed junction integrity in *aka* mutants by transmission EM. Lack of individual SJ components is associated with reduced or absent electron-dense septa (Lamb et al., 1998; Behr et al., 2003; Wu et al., 2004; Furuse and Tsukita, 2006). In stage 16 *aka* embryos, SJ septa spanning the space between two neighboring cells were present in the BCJ region

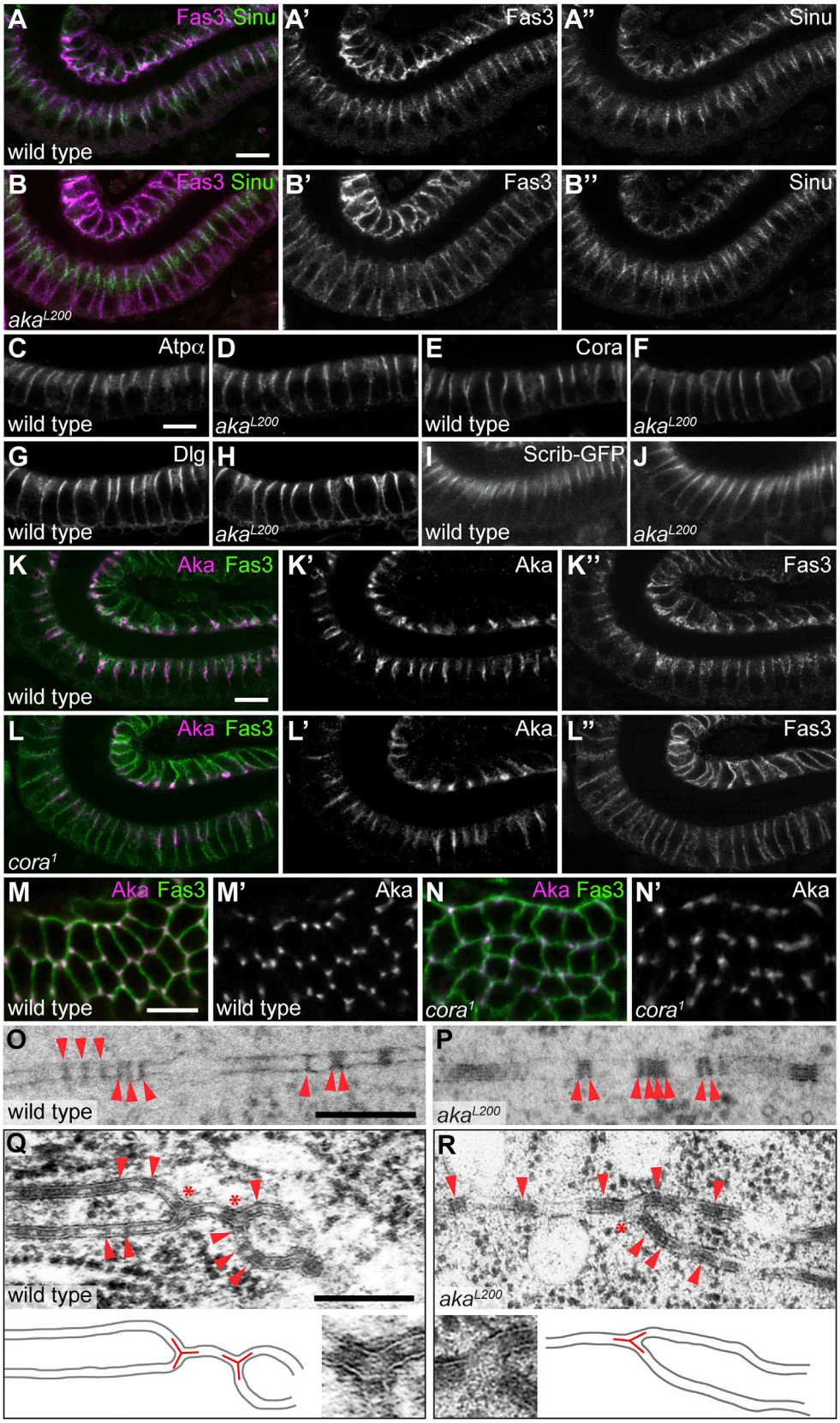


(legend on next page)

(Figures 4O and 4P), although SJs appeared to disintegrate in later (stage 17) embryos, possibly as a consequence of defects in cell adhesion or epithelial barrier formation. We also analyzed TCJs, which are visible as bifurcations of the BCJs. In wild-type embryos, the dihedral angles of the three adjoining cell membranes were equal (120 degrees) around the bifurcation (Figure 4Q; Figures S4A–S4C; Graf et al., 1982). Three bicellular limiting strands were described to delineate the TCJ space that contains a row of stacked diaphragms appearing as electron-dense material (Graf et al., 1982). In *aka* embryos, bicellular septa were present near TCJs, but the central TCJ space always lacked electron-dense material and the dihedral angles of the converging membranes were frequently unequal (Figure 4R). Consistent with these observations in *aka* embryos, RNAi-mediated depletion of Aka from wing imaginal disc cells led to a broader distribution of TCJ angles compared to control cells (Figures S4D–S4L). Together, these findings suggest that Aka is required specifically for the formation and correct geometry of TCJs, whereas bicellular SJ assembly is independent of *aka* function.

## Aka Is Necessary and Sufficient for Accumulation of Gliotactin at Tricellular Junctions

To address Aka's role in TCJ formation, we asked whether Aka and Gli depend on each other for their ability to accumulate at TCJs. Whereas Aka and Gli co-localized at TCJs in the wild-type (Figure 5A), TCJ accumulation of Gli was lost in *aka* mutant epithelia (Figure 5C). Instead, Gli was uniformly distributed around the cell circumference (Figure 5C′), although it remained enriched at the apico-lateral SJ domain (Figures S5C and S5D). In contrast, Aka still accumulated at TCJs in *Gli* mutants (Figure 5B). We also analyzed the distribution of Gli-YFP in larvae, in which we depleted Aka from stripes of cells by RNAi (Figures S5A and S5B). In control epidermal and wing imaginal disc cells, Gli-YFP accumulated at TCJs and was present at low levels at BCJs. In adjacent cells expressing *aka* dsRNA, Gli-YFP accumulation at TCJs was lost, whereas Gli-YFP signals at BCJs increased, consistent with re-distribution of Gli-YFP from TCJs to BCJs upon depletion of Aka. These findings suggest that Aka acts upstream of Gli in TCJ assembly.

In wild-type embryos, Gli is initially distributed throughout lateral membranes and begins to accumulate at TCJs during late stage 13 (Schulte et al., 2003). Strikingly, mis-expressing Aka in epidermal stripes before the onset of endogenous *aka* expression was sufficient to initiate premature TCJ accumulation of Gli at early stage 13 (Figure 5D), indicating that Aka is limiting for TCJ localization of Gli. However, Gal4-driven overexpression led to accumulation of Aka outside of TCJs, but was not able to direct Gli to ectopic locations. Thus, Aka appears to associate with Gli only in the context of TCJs. Together, these results suggest that Aka acts early in TCJ assembly by recruiting or maintaining Gli at tricellular vertices.

## Aka's PDZ-Binding Motif Is Not Required for Maintaining Aka and Gli Localization at TCJs

To understand how Aka localizes to tricellular vertices, we investigated the contributions of Aka's extracellular and cytoplasmic parts to TCJ localization. We used Tobacco Etch Virus (Tev) protease to release the Aka C terminus including the PDZ-binding motif by cleaving the Aka-Ty1-Tev-SGFP-FLAG protein between the Ty1 and SGFP tags (Figure 6A). Membrane-tethered Tev protease was expressed in epidermal stripes of *aka* embryos carrying Aka-Ty1-Tev-SGFP-FLAG as the only source of Aka protein (Figure 6B). In Tev-expressing cells, the C-terminal fragment carrying the SGFP tag became diffusely localized or degraded, whereas in the same cells the N-terminal fragment with the Ty1 tag remained localized at TCJs (Figures 6B and 6C). Similarly, TCJ accumulation of Gli remained unchanged upon Tev-mediated release of the Aka C terminus (Figure 6D). However, we cannot rule out that incomplete Tev protease cleavage might leave an undigested fraction of Aka-Ty1-Tev-SGFP-FLAG protein that could support TCJ formation. We therefore generated a mutant Aka version lacking the PDZ-binding motif (UAS-Aka-ΔPDZB) and tested its function in *aka* embryos. Strikingly, Aka-ΔPDZB rescued tracheal defects (Figure 1E) and accumulation of Gli at TCJs in salivary glands (Figures 6H–6J), although Fas3 was still mislocalized (Figures 6E–6G). Together, these results indicate that Aka's C terminus, including the PDZ-binding motif, is not required to maintain TCJ localization of Aka's extracellular part and of Gli.

The absence in the C-terminal part of conserved stretches other than the PDZ-binding motif suggested that Aka may be targeted to TCJs by cues outside the cytoplasmic domain. To test whether extracellular interactions between Aka proteins residing

**Figure 4. Localization of Aka and of Septate Junction Proteins Are Mutually Independent**

(A and B) Wild-type and $aka^{L200}$ embryos labeled for Fas3 (magenta) and Sinu (green). Fas3 and Sinu localize to the apical-most third of the lateral membrane in the hindgut epithelium (A–A″). In $aka^{L200}$ mutants, Fas3 is mislocalized and distributes along the entire lateral cell surface, whereas Sinu retains its normal apico-lateral localization (B–B″).

(C–H) Wild-type and $aka^{L200}$ embryos labeled for ATPα (C and D), Cora (E and F) or Dlg (G and H). The three SJ components show similar apico-lateral localization in the hindgut of wild-type (C, E, and G) and *aka* (D, F, and H) embryos.

(I and J) Images of living embryos show apico-lateral localization of Scrib-GFP in wild-type (I) and *aka* mutant (J) hindgut epithelium.

(K–N) Wild-type and $cora^{1}$ embryos labeled for Aka (magenta) and Fas3 (green). Fas3 and Aka accumulate apico-laterally in wild-type hindgut (K–K″). In *cora* mutants, Aka localization is similar to that observed in the wild-type, whereas Fas3 is detected along the entire lateral cell surface (L–L″). En face view shows that Aka localizes to TCJs in the wild-type (M and M′) and $cora^{1}$ mutant (N and N′) hindgut. All embryos were at early stage 16.

(O–R) Transmission EM micrographs of epidermis in stage 16 (O and P; sectioned along apical-basal axis) and stage 17 (Q and R; sectioned parallel to apical surface) embryos. Note that bicellular SJ septa (red arrowheads) are present in wild-type (O and Q) and $aka^{L200}$ (P and R) embryos. For (Q) and (R), schematic drawings indicate the course of the plasma membrane. Small insets show close-ups of TCJs. Electron-dense material in the TCJ center is absent from TCJs in *aka* mutants. Also note that the dihedral angles of bicellular membranes are equal (120 degrees, indicated by red stars in bottom images) close to the TCJ in the wild-type, whereas angles are unequal in the *aka* mutant.

Scale bars represent 5 μm (A–N), 200 nm (O and P), and 250 nm (Q and R).

See also Figures S3 and S4.

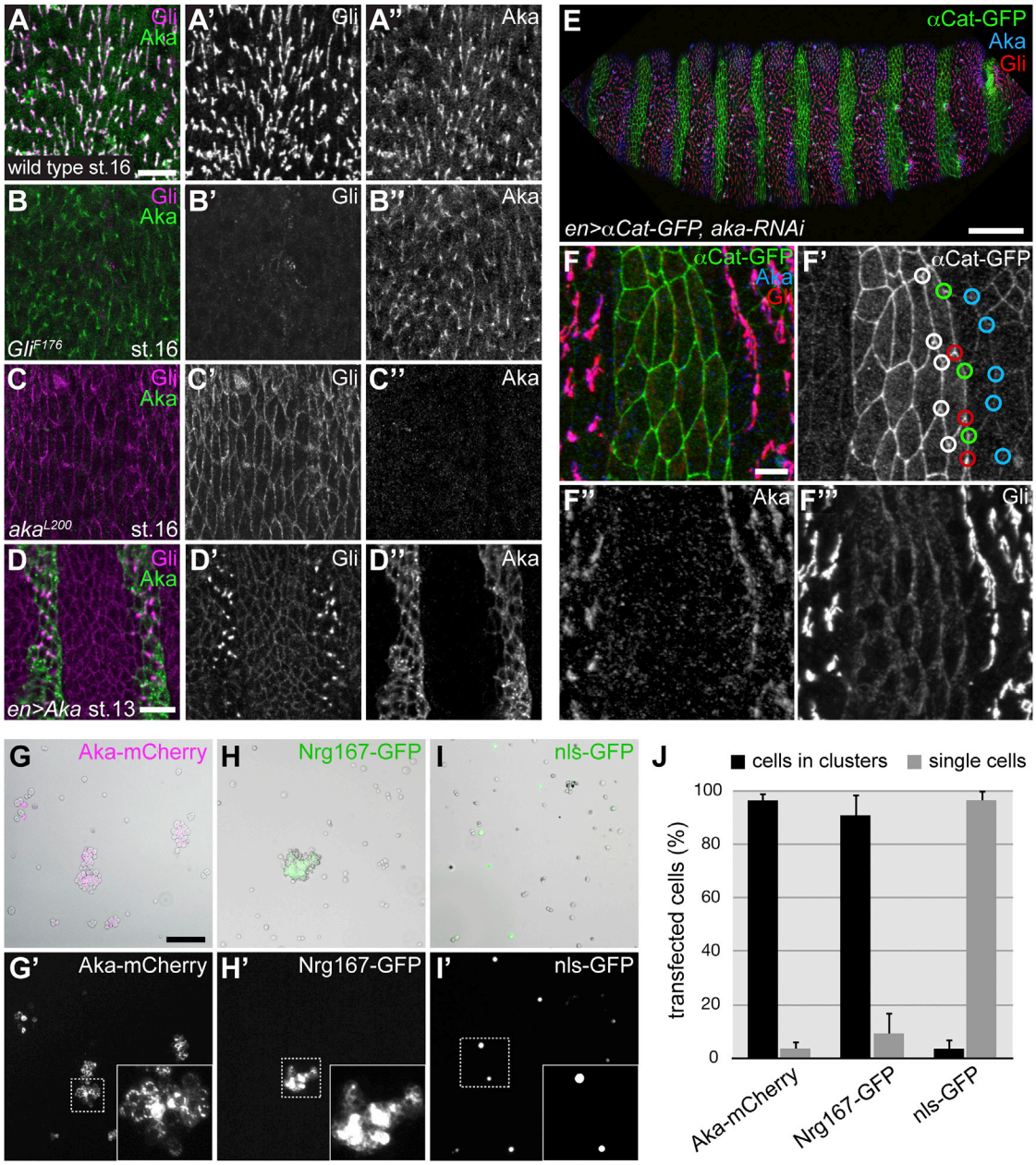


**Figure 5. Aka Is Necessary and Sufficient for Accumulation of Gliotactin at Tricellular Junctions and Mediates Adhesion in S2 Cells**

(A–C) *En face* view of epidermis in stage 16 embryos labeled with Anti-Gli (magenta) and anti-Aka (green). Aka and Gli accumulate at TCJs in the wild-type (A). Aka also accumulates at TCJs in *Gli* embryos, in which Gli is not detectable (B). In *aka*-mutant embryos, Gli fails to accumulate at TCJs, but spreads along BCJs (C).

(D) *En face* view of epidermis in early stage 13 wild-type embryo labeled with Anti-Gli (magenta) and anti-Aka (green). Aka was expressed prematurely in epidermal stripes under the control of *en*-Gal4. Prior to the onset of endogenous Aka expression, Gli is distributed along BCJs. Note that in cells that express Aka prematurely Gli accumulates at TCJs.

(E) Stage 16 embryo expressing αCat-GFP (green) and $aka^{RNAi}$ under the control of *en*-Gal4. Gli (red) fails to accumulate at TCJs in $aka^{RNAi}$-expressing stripes of cells, from which Aka (blue) is depleted.

(F–F‴) Close-up of epidermis as in (E). Gli (F‴, red in F) accumulates at TCJs in unperturbed control cells, whereas Gli distributes along BCJs in $aka^{RNAi}$-expressing cells marked by αCat-GFP. Aka (blue in F) is depleted from $aka^{RNAi}$-expressing cells (F′). Note that Aka and Gli accumulate at TCJs only when Aka expression in all three cells abutting a TCJ is unperturbed (blue circles in F′), whereas Aka and Gli accumulation at TCJs is lost when Aka is depleted from one (green circles), two (red circles), or all three (white circles) cells adjoining a three-cell vertex.

(G–I′) S2 cells were transfected with Aka-mCherry (magenta; G), Nrg167-GFP (green; H), or nlsGFP (green; I) constructs. Cells expressing Aka-mCherry or Nrg167-GFP, but not nlsGFP-expressing cells, form aggregates. (G and H) are bright-field images overlaid with epifluorescence images shown in (G′–I′). Insets show close-up views of cells marked by boxes in (G′–I′). Note that cell clusters in (G) consist of Aka-mCherry-expressing cells only and do not include non-transfected cells, suggesting that Aka mediates homophilic adhesion.

*(legend continued on next page)*

on adjacent cells could be involved in TCJ localization, we analyzed the distribution of Aka and Gli in mosaic situations where Aka was depleted from one or two cells abutting a three-cell vertex by RNAi (Figure 5E; Figure S5B). Interestingly, TCJ accumulation of Aka and Gli depends on Aka expression in all three adjoining cells because Aka and Gli failed to accumulate at TCJs in situations where Aka was depleted from one or two of the cells (Figures 5F–5F‴; Figure S5B). This finding suggests that the extracellular domains of Aka molecules produced by different cells interact with each other. Consistent with this idea, S2 cells transfected with an Aka-mCherry construct formed aggregates (Figures 5G–5J). Although we were not able to detect enrichment of Aka-mCherry at tricellular contacts in S2 cell aggregates, possibly due to the high expression levels upon transfection, these results indicate that Aka can mediate homophilic adhesion.

To explore if the geometry of tricellular vertices may theoretically suffice as cue to promote TCJ localization of Aka via extracellular interactions, we performed computer simulations. At TCJs, Aka molecules from different cells might form complexes, and such complexes are automatically contained to one instead of two dimensions (Figure 7C). A reduction of dimensionality can lead to increased binding rates (Adam and Delbrück, 1968; Richter and Eigen, 1974). Simulating this effect revealed a 40-fold enrichment of Aka at TCJs compared to BCJs after 2–2.5 hr of simulated time (Figure 7D; Figure S1; Movie S1). However, this equilibrium was sensitive to parameter changes (see Supplemental Experimental Procedures). Thus, enrichment through self-assembly at TCJs may in principle emerge from the geometry of tricellular vertices combined with the capacity of a protein to multimerize, although additional factors are likely to be involved. Together, our findings suggest that TCJ localization results from the geometry of three-cell vertices and from Aka's intrinsic protein features, rather than from a TCJ-directed intracellular transport pathway.

## DISCUSSION

Ultrastructural analyses revealed a unique junctional architecture at points in epithelia where three cells meet. Yet, only few TCJ-specific proteins are known, and how they assemble into a tightly localized complex exclusively at tricellular vertices is not understood. Here we describe a transmembrane protein that plays a critical role in TCJ assembly and epithelial barrier formation. First, we show that Aka localizes to TCJs in ectodermal and endodermal epithelia, suggesting that Aka is a core TCJ component. Second, we demonstrate that Aka is specifically required for the assembly and correct geometry of tricellular, but not of bicellular SJs, and that Aka localizes to TCJs independently of bicellular SJs. Third, Aka is required for recruiting or maintaining Gli, the only other invertebrate TCJ component characterized so far, at tricellular vertices. Conversely, Gli is not required for TCJ localization of Aka. Fourth, Aka mis-expression causes premature accumulation of Gli at TCJs, indicating that Aka acts upstream of Gli in initiating TCJ formation.

Aka protein contains a large extracellular domain with a conserved tripartite repeat structure. This unique structure distinguishes Aka from other known TCJ proteins. Tricellulin, a four-pass transmembrane protein in vertebrates, localizes to the central sealing elements, suggesting that it participates in the specialized bicellular contacts that surround each three-cell vertex (Ikenouchi et al., 2005). Tricellulin is recruited to TCJs by the immunoglobulin domain transmembrane protein LSR, but how LSR localizes to TCJs is still unclear (Masuda et al., 2011). In *Drosophila*, Gli, a transmembrane protein with a cholinesterase domain lacking catalytic activity, accumulates at TCJs, but is also involved in bicellular SJ organization (Genova and Fehon, 2003; Schulte et al., 2003). Phosphorylation-dependent endocytic turnover and indirect association with Dlg are required for accumulation of Gli at TCJs (Schulte et al., 2006; Padash-Barmchi et al., 2010, 2013). However, the mechanisms underlying TCJ-specific localization are not understood for Gli or any other TCJ protein.

Our results suggest that Aka acts at an early step during TCJ assembly by recruiting other TCJ components, including Gli, to tricellular vertices. TCJ localization of Aka and Gli does not require Aka's C terminus, including the PDZ-binding motif. Similarly, Gli was found to localize to TCJs independently of its PDZ-binding motif (Schulte et al., 2006). These findings suggest that Aka and Gli might be targeted to TCJs through their extracellular domains, rather than through a cytoplasmic localization machinery. Because mislocalized Aka protein is not sufficient to recruit Gli to ectopic locations, Aka might not interact directly with Gli, or only do so in the context of TCJs. Consistent with this notion, we were not able to detect co-immunoprecipitation of Aka and Gli (not shown). Interestingly, overexpression of Gli (Schulte et al., 2006) or absence of Aka causes Gli to spread from TCJs to BCJs. Thus, Gli does not have an intrinsic propensity to localize to TCJs, but by default localizes to the apicolateral membrane domain occupied by SJs along the cell perimeter. TCJ accumulation of Gli therefore requires (1) association with the apicolateral membrane and (2) Aka-dependent recruitment of Gli specifically to TCJs. Our findings show that unlike Gli, Aka does not depend on bicellular SJs for its localization to TCJs, and suggest that Aka protein might have intrinsic properties that lead to its accumulation at TCJs.

Tricellular vertices display a unique geometry where three plasma membranes are in close proximity and at fixed angles (Figures 7A and 7B). The exceptional curvature of the plasma membrane at these sites implies distinct physical properties compared to bicellular contacts. Intriguingly, we found that TCJ assembly depends on Aka expression in all three cells adjoining a vertex, suggesting that extracellular interactions between Aka molecules from different cells are essential for TCJ formation. Considering the size of Aka's extracellular domain (303 kDa), it is likely that a single Aka protein spans the entire TCJ canal (25–30 nm; Graf et al., 1982; Noirot-Timothée et al., 1982), although shorter Aka isoforms may constitute different

(J) Quantification of cell aggregation. Bars show the percentage of transfected cells (positive for GFP or mCherry, respectively) found in aggregates or as single cells, respectively. Error bars indicate SD of two replicates. n = 188 (Aka-mCherry); n = 150 (Nrg167-GFP); n = 400 (nls-GFP).
Scale bars represent 10 μm (A–C, D); 50 μm (E); 5 μm (F–F‴); 100 μm (G–I′).
See also Figure S5.

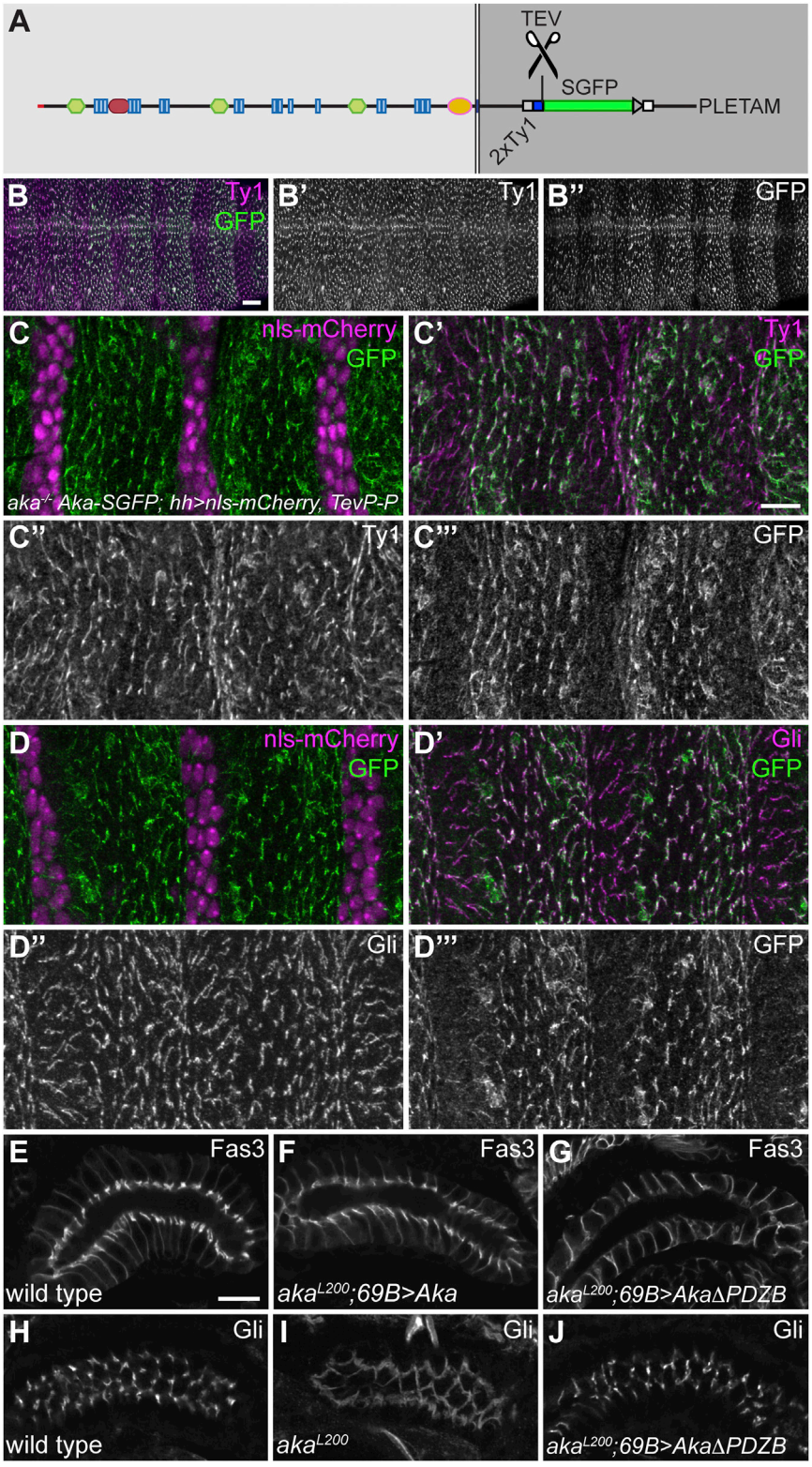


**Figure 6. The Aka C Terminus Is Not Required for Maintaining TCJ Localization of Aka's Extracellular Part and of Gliotactin**

(A) Structure of the Aka-Ty1-Tev-SGFP-FLAG construct. Positions of the 2xTy1 epitope tag, the Tev protease cleavage site (TEV), the superfolder GFP (SGFP) sequence, and the C-terminal PDZ-binding motif (PLETAM) are indicated (not drawn to scale with the rest of the protein).

(B) Confocal section of an embryo expressing Aka-Ty1-Tev-SGFP-FLAG as the only source of Aka protein. Prenylated Tev protease (UAS-TevP-P) is expressed in epidermal stripes under the control of *hh*-Gal4. N- and C-terminal portions of Aka were detected by anti-Ty1 and anti-GFP staining, respectively. Note that GFP staining is severely reduced in segmental stripes (B″), whereas Ty1 staining is unchanged along the embryo (B′).

(C and D) Close-up views of embryonic epidermis as in (B) with Tev-expressing cells marked by co-expression of nls-mCherry. The C-terminal Aka fragment detected with anti-GFP becomes diffusely localized or degraded in Tev-expressing cells, whereas the Aka N-terminal fragment detected by anti-Ty1 staining (C″), as well as Gli (D″), remain localized at TCJs.

(E–J) Salivary glands from stage 16 embryos labeled for Fas3 (E–G) or Gli (H–J; en face view). 69B-Gal4 was used to drive expression of Aka (UAS-Aka; F) or of an Aka variant lacking the C-terminal PDZ-binding motif (UAS-AkaΔPDZB, G and J) in salivary glands. Fas3 localizes apicolaterally in wild-type (E) and in *aka* embryos expressing Aka (F), but is mislocalized along the entire lateral membrane in *aka* embryos expressing AkaΔPDZB (G). Gli localizes to TCJs in the wild-type (H) and along BCJs in *aka* embryos (I). Expression of AkaΔPDZB is sufficient to restore Gli accumulation at TCJs in salivary glands (J).

Scale bars represent 20 μm (B), 10 μm (C and D), and 5 μm (E–J).

structures. Shorter Aka species might carry out functions that may or may not be related to the function of full-length Aka at TCJs. Alternatively, Aka fragments may reflect turnover of TCJ complexes, e.g., during junctional remodeling.

It is tempting to speculate that the three repeat regions in full-length Aka protein, with apparent similar domain organization, could make equal contacts with the three cell corners in the plane perpendicular to the central TCJ canal. Possibly, interaction with membrane components in the tricellular region occurs via the three SR domains, since such domains are found in receptors that recognize a wide range of molecular patterns, including surface proteins, carbohydrates, lipids, lipopolysaccharides, and peptidoglycans associated with pathogens or apoptotic cells (Bowdish and Gordon, 2009). Because such three-way contacts may, for steric reasons, only be possible at vertices, they might selectively stabilize Aka complexes at these sites. Our computer simulations suggest that the enrichment of Aka at three-cell vertices could

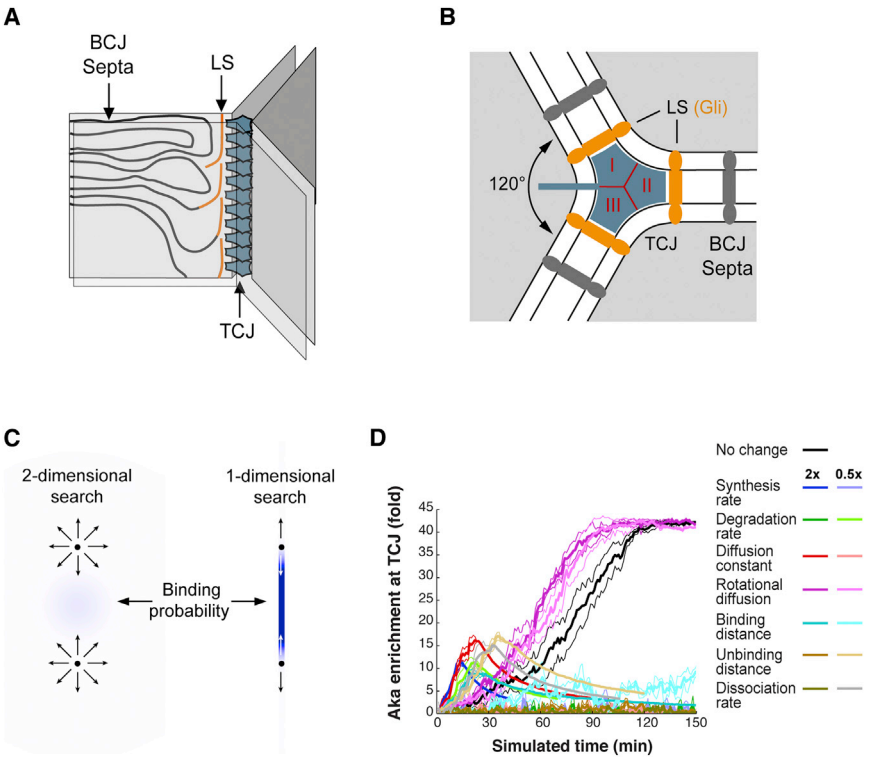


**Figure 7. The Geometry of Three-Cell Vertices May Promote Accumulation of Aka at TCJs**

(A) Schematic drawing of a three-cell vertex based on freeze-fracture electron micrographs (Graf et al., 1982). Plasma membranes of three adjoining cells are shown. Bicellular SJ septa are shown for one cell only. Near the tricellular junction (TCJ), bicellular SJ septa turn by 90 degrees to run along the apical-basal axis, forming the lateral limiting strands (LS, orange). Stacked triangular diaphragms in the TCJ central canal contact membrane corners and the three limiting strands on each side of the TCJ.

(B) Schematic view of cross-section at a three-cell vertex (adapted from Graf et al., 1982). BCJ septa are indicated in dark gray, TCJ limiting strands (LS) in orange. Gli was proposed to be associated with the limiting strands (Schulte et al., 2003). Note that dihedral angles between bicellular membranes approaching the TCJ are equal. The size and triple-repeat structure of Aka's extracellular domain suggest that the triangular diaphragms in the central canal (Graf et al., 1982) may contain Aka protein (triangular structure inside TCJ canal).

(C) The geometry of tricellular vertices could promote Aka accumulation by confining diffusion at the TCJ to one dimension (compared to two dimensions in the rest of the membrane), which can increase the probability of interaction between binding partners.

(D) Computer simulations of Aka enrichment at TCJs in the absence of external cues. The model includes synthesis, degradation, binding, dissociation, and diffusion within the plasma membrane. Aka enrichment at TCJs over time is plotted. Different colors show sensitivity to halving and doubling parameters indicated in the legend to the right. Results are mean (fat lines) ± SEM (narrow lines) from three independent simulations. Note that Aka becomes enriched 40-fold at TCJs after 2–2.5 hr of simulated time, although this equilibrium is sensitive to changing parameters by 2-fold.

See also Movie S1, Figure S6, and Supplemental Experimental Procedures for details.

theoretically be enhanced by the reduction of dimensionality in the tricellular region, which may promote stacking interactions between Aka molecules within the central TCJ canal. This idea is consistent with the regular structure of the TCJ diaphragms and the equal dihedral angles near TCJs as observed with electron microscopy (Fristrom, 1982; Graf et al., 1982; Noirot-Timothée et al., 1982). Stacking might occur with Aka molecules rotated by 120 or 240 degrees within the stack, perhaps in a helical array, depending on the contributing cell (Figure S6H). Notably, such a scenario would explain our finding that TCJ formation requires Aka protein production by all three cells adjoining a vertex. A high priority of future studies will be to investigate the arrangement of Aka proteins at TCJs. Together, our results on Aka localization, the geometry of three-cell vertices, and the triple-repeat structure of Aka protein suggest a mechanism of TCJ formation, which is promoted by self-assembly of Aka at tricellular contacts. Such self-assembly might additionally involve interactions with other membrane-associated or extracellular components, and could cooperate with bicellular adhesion molecules that zip up bicellular contacts. It will be interesting to test whether the geometry of tricellular vertices and the specific properties of Aka protein are sufficient to direct its accumulation to TCJs. Conversely, perturbed TCJ geometry upon loss of Aka may have long-range effects, such as the loss of cell-cell adhesion that we observed in late-stage *aka* embryos. Interestingly, depletion of Tricellulin from mammalian cells affects cell shape and the F-actin network, suggesting that TCJs may in fact have organizing activity on the entire cell (Oda et al., 2014).

The existence of *aka* homologs in invertebrates and cephalochordates correlates with the presence of SJs in these groups (Banerjee et al., 2006). However, the proposed self-assembly model for TCJ formation in *Drosophila* may apply also to vertebrates, although the corresponding proteins remain to be discovered. A better understanding of TCJ assembly will be a key step toward elucidating how these poorly characterized cellular structures provide epithelial barrier function, while at the same time allowing the passage of migrating lymphocytes, metastatic cells, and intracellular pathogens.

## EXPERIMENTAL PROCEDURES

### Genetics

Fly stocks are described in FlyBase unless mentioned otherwise: *aka*$^{YD1046}$ (Quiñones-Coello et al., 2007), *Df(2L)Exel6009*, *Df(2L)BSC171*, *CyO Dfd-YFP*, *btl*-Gal4, *en*-Gal4, *hh*-Gal4, *69B*-Gal4, *UAS-mCherry-nls*, *UAS-Verm-mRFP*, *UAS-α-Catenin-GFP*, *DE-Cad-mTomato*, *UAS-TevP-P* (prenylated Tev protease; gift from Marko Brankatschk, Dresden, Germany), *cora*$^{1}$, *Mcr*$^{K103}$, *Nrg*$^{17}$, *sinu*$^{06524}$, *UAS-lacZ*$^{RNAi}$, *UAS-dicer2* (VDRC-60014), *Dlg-GFP* (YC0005), *Scrib-GFP* (CA07683), *Nrx-IV-GFP* (CA06597; Quiñones-Coello et al., 2007), *Gli-YFP* (CPTI-002805), *Lac-YFP* (CPTI-002601), and *Nrg-YFP* (CPTI-001714; Lowe et al., 2014). For tracheal-specific RNAi, *UAS-aka*$^{RNAi}$ (VDRC-52608) and *UAS-dicer2* were co-expressed using *btl*-Gal4. *aka* and

*Gli* mutations were induced by ethylmethanesulfonate (EMS) mutagenesis (see Supplemental Experimental Procedures). *Gli* alleles were $Gli^{dv3}$ (Schulte et al., 2003), $Gli^{AE2\ delta45}$ (Auld et al., 1995), $Gli^{F156}$, and $Gli^{F176}$ (this work). $Gli^{F156}$ has a deletion of a single nucleotide (C3893), resulting in a frame shift and a premature stop codon after 476 aa within the cholinesterase domain. $Gli^{F176}$ has a C4901 > T transition, resulting in a premature stop codon after 724 aa within the transmembrane domain.

### Antibodies and Immunostainings

Embryos were fixed in 4% formaldehyde in PBS/heptane for 20 min and devitellinized by shaking in methanol/heptane. Embryos for anti-Aka immunostainings were heat-fixed. Antibodies were chicken anti-GFP (1:500, Abcam), mouse anti-GFP (1:300; Clontech), mouse anti-Cora (1:20; Lamb et al., 1998), mouse anti-Gli 1F6 (1:200; Auld et al., 1995), mouse anti-Dlg 4F3 (1:500; DSHB), mouse anti-Fas3 7G10 (1:50; DSHB), mouse anti-TY1 BB2 (1:500; Sigma), mouse anti-Arm N27A1 (1:7, DSHB), rat anti-HA 3F10 (1:300; Roche), rabbit anti-Lgl (1:200; Santa Cruz), rabbit anti-Sinu (1:500; Wu et al., 2004), and guinea pig anti-Mtf (1:500; Tiklová et al., 2010). Goat secondary antibodies were conjugated with Alexa 405, Alexa 488, Alexa 568 (Molecular Probes), or Cy5 (Jackson ImmunoResearch). Chitin was detected using Alexa-Fluor-SNAP-tagged chitin-binding domain from *Bacillus circulans* chitinase A1 prepared as described (Caviglia and Luschnig, 2013). The anti-Aka antiserum was generated by GenScript by immunizing rabbits with the peptide CRTEGGTPAGRRGQP (corresponding to aa 2933-2946 in Aka-PB). The antiserum was affinity-purified and used at a dilution of 1:500 for immunostainings.

### Immunoblotting

Lysates were prepared by homogenizing 200 embryos (stage 14–16) in 100 µl sample buffer (Invitrogen). Extracts were heated at 70°C for 5 min before loading on Novex NuPAGE 4%–12% Bis-Tris gels (Life Technologies) and blotting onto PVDF membranes (pore size 0.2 µm, Millipore). Primary antibodies (rabbit anti-Aka [1:10,000], mouse anti-α-tubulin [1:10,000; Sigma]) were detected with HRP-conjugated secondary antibodies (1:2,500; Cell Signaling) and ECL+ (Pierce).

### Dextran Injections

Rhodamine-labeled dextran (10 kDa; Molecular Probes) was injected as described elsewhere (Lamb et al., 1998) into wild-type and $aka^{L200}$ embryos carrying *btl-Gal4 UAS-GFP* to label tracheal cells. Embryos were imaged 20 min after injection.

### Cell Aggregation Assay

*Drosophila* S2 cells were cultured in Schneider's medium (Invitrogen) at 27°C. Cells were transfected with pUASTattB-Aka-mCherry, pUAST-Nrg167-GFP (positive control; D. Siegenthaler, E. Moreno and J. Pielage, personal communication), or pUbi-nlsGFP (negative control). pCaSpeR4-Act5c-GAL4 was co-transfected to drive expression of UAS constructs. 800,000 cells were transfected with 1 µg plasmid DNA using FuGene HD transfection reagent (Invitrogen). After three days, cells were dissociated by repeated pipetting. Density was adjusted to $1 \times 10^6$ cells/ml with Schneider's medium; 0.5 ml cell suspension was shaken for 2.5 hr at 100 rpm in an Eppendorf tube at room temperature. To analyze aggregation, cells were spotted on a slide and observed using epifluorescence/DIC. The number of transfected (GFP- or mCherry-positive) single cells and cells in clusters (containing at least three cells) was determined by manual counting. Transfections were performed in duplicate.

## SUPPLEMENTAL INFORMATION

Supplemental Information includes Supplemental Experimental Procedures, six figures, and one movie and can be found with this article online at http://dx.doi.org/10.1016/j.devcel.2015.03.023.

## AUTHOR CONTRIBUTIONS

All authors designed and conducted experiments and analyzed the data. T.A.W. performed computer simulations and wrote corresponding sections of the text. A.U. and S.L. wrote the manuscript.

## ACKNOWLEDGMENTS

We are indebted to Kristina Armbruster and Stefanie Limmer, who isolated *aka* mutants. We thank Markus Affolter, Vanessa Auld, Marko Brankatschk, Rick Fehon, Jan Pielage, Frank Schnorrer, Pavel Tomancak, the Bloomington and Kyoto *Drosophila* Stock Centers, the Vienna *Drosophila* Resource Center, and the Developmental Studies Hybridoma Bank for providing fly stocks and reagents. The Centre for Cellular Imaging and the Proteomics Core Facility, both at GU, provided support with confocal imaging and protein identification. The electron microscopy unit at GU and the Center for Microscopy and Image Analysis at UZH provided support with electron microscopy. We thank Dominique Förster and Martina Trost for help with experiments, Mark Robinson and Benjamin Risse for advice on statistics, Riccardo Murri and Antonio Messina (Grid Computing Competence Center, UZH) for computer support, and Daniel Wechsler, Tobias Grubenmann, Prasenjit Saha, and Christof Aegerter for discussions. S.L. would like to thank Christian Lehner for continuous support and discussions. J.G. was supported by a Forschungskredit fellowship of the UZH. Work in A.U.'s laboratory was supported by the Swedish Cancer Society and the University of Gothenburg. Work in S.L.'s laboratory was supported by the Swiss National Science Foundation (SNF ProDoc_PDFMP3_127362, SNF 31003A_141093_1), the University of Zürich, and the Kanton Zürich.

Received: September 21, 2014
Revised: February 9, 2015
Accepted: March 26, 2015
Published: May 14, 2015

## REFERENCES

Adam, G., and Delbrück, M. (1968). Reduction of dimensionality in biological diffusion processes. In Structural Chemistry and Molecular Biology, A. Rich and N. Davidson, eds. (W.H. Freeman and Co.).

Auld, V.J., Fetter, R.D., Broadie, K., and Goodman, C.S. (1995). Gliotactin, a novel transmembrane protein on peripheral glia, is required to form the blood-nerve barrier in Drosophila. Cell *81*, 757–767.

Banerjee, S., Sousa, A.D., and Bhat, M.A. (2006). Organization and function of septate junctions: an evolutionary perspective. Cell Biochem. Biophys. *46*, 65–77.

Banerjee, S., Bainton, R.J., Mayer, N., Beckstead, R., and Bhat, M.A. (2008). Septate junctions are required for ommatidial integrity and blood-eye barrier function in Drosophila. Dev. Biol. *317*, 585–599.

Bätz, T., Förster, D., and Luschnig, S. (2014). The transmembrane protein macroglobulin complement-related is essential for septate junction formation and epithelial barrier function in Drosophila. Development *141*, 899–908.

Behr, M., Riedel, D., and Schuh, R. (2003). The claudin-like megatrachea is essential in septate junctions for the epithelial barrier function in Drosophila. Dev. Cell *5*, 611–620.

Bilder, D., and Perrimon, N. (2000). Localization of apical epithelial determinants by the basolateral PDZ protein Scribble. Nature *403*, 676–680.

Bowdish, D.M., and Gordon, S. (2009). Conserved domains of the class A scavenger receptors: evolution and function. Immunol. Rev. *227*, 19–31.

Burns, A.R., Walker, D.C., Brown, E.S., Thurmon, L.T., Bowden, R.A., Keese, C.R., Simon, S.I., Entman, M.L., and Smith, C.W. (1997). Neutrophil transendothelial migration is independent of tight junctions and occurs preferentially at tricellular corners. J. Immunol. *159*, 2893–2903.

Caviglia, S., and Luschnig, S. (2013). The ETS domain transcriptional repressor Anterior open inhibits MAP kinase and Wingless signaling to couple tracheal cell fate with branch identity. Development *140*, 1240–1249.

Chakraborty, P., William Buaas, F., Sharma, M., Smith, B.E., Greenlee, A.R., Eacker, S.M., and Braun, R.E. (2014). Androgen-dependent sertoli cell tight junction remodeling is mediated by multiple tight junction components. Mol. Endocrinol. *28*, 1055–1072.

Förster, D., Armbruster, K., and Luschnig, S. (2010). Sec24-dependent secretion drives cell-autonomous expansion of tracheal tubes in Drosophila. Curr. Biol. *20*, 62–68.

Fristrom, D.K. (1982). Septate junctions in imaginal disks of Drosophila: a model for the redistribution of septa during cell rearrangement. J. Cell Biol. *94*, 77–87.

Fukumatsu, M., Ogawa, M., Arakawa, S., Suzuki, M., Nakayama, K., Shimizu, S., Kim, M., Mimuro, H., and Sasakawa, C. (2012). Shigella targets epithelial tricellular junctions and uses a noncanonical clathrin-dependent endocytic pathway to spread between cells. Cell Host Microbe *11*, 325–336.

Furuse, M., and Tsukita, S. (2006). Claudins in occluding junctions of humans and flies. Trends Cell Biol. *16*, 181–188.

Furuse, M., Izumi, Y., Oda, Y., Higashi, T., and Iwamoto, N. (2014). Molecular organization of tricellular tight junctions. Tissue Barriers *2*, e28960.

Genova, J.L., and Fehon, R.G. (2003). Neuroglian, Gliotactin, and the Na+/K+ ATPase are essential for septate junction function in Drosophila. J. Cell Biol. *161*, 979–989.

Graf, F., Noirot-Timothée, C., and Noirot, C. (1982). The specialization of septate junctions in regions of tricellular junctions. I. Smooth septate junctions (=continuous junctions). J. Ultrastruct. Res. *78*, 136–151.

Higashi, T., Tokuda, S., Kitajiri, S., Masuda, S., Nakamura, H., Oda, Y., and Furuse, M. (2013). Analysis of the 'angulin' proteins LSR, ILDR1 and ILDR2—tricellulin recruitment, epithelial barrier function and implication in deafness pathogenesis. J. Cell Sci. *126*, 966–977.

Ikenouchi, J., Furuse, M., Furuse, K., Sasaki, H., Tsukita, S., and Tsukita, S. (2005). Tricellulin constitutes a novel barrier at tricellular contacts of epithelial cells. J. Cell Biol. *171*, 939–945.

Izumi, Y., Yanagihashi, Y., and Furuse, M. (2012). A novel protein complex, Mesh-Ssk, is required for septate junction formation in the Drosophila midgut. J. Cell Sci. *125*, 4923–4933.

Jaspers, M.H., Nolde, K., Behr, M., Joo, S.H., Plessmann, U., Nikolov, M., Urlaub, H., and Schuh, R. (2012). The claudin Megatrachea protein complex. J. Biol. Chem. *287*, 36756–36765.

Kelley, L.A., and Sternberg, M.J. (2009). Protein structure prediction on the Web: a case study using the Phyre server. Nat. Protoc. *4*, 363–371.

Krug, S.M., Amasheh, S., Richter, J.F., Milatz, S., Günzel, D., Westphal, J.K., Huber, O., Schulzke, J.D., and Fromm, M. (2009). Tricellulin forms a barrier to macromolecules in tricellular tight junctions without affecting ion permeability. Mol. Biol. Cell *20*, 3713–3724.

Lamb, R.S., Ward, R.E., Schweizer, L., and Fehon, R.G. (1998). Drosophila coracle, a member of the protein 4.1 superfamily, has essential structural functions in the septate junctions and developmental functions in embryonic and adult epithelial cells. Mol. Biol. Cell *9*, 3505–3519.

Llimargas, M., Strigini, M., Katidou, M., Karagogeos, D., and Casanova, J. (2004). Lachesin is a component of a septate junction-based mechanism that controls tube size and epithelial integrity in the Drosophila tracheal system. Development *131*, 181–190.

Lowe, N., Rees, J.S., Roote, J., Ryder, E., Armean, I.M., Johnson, G., Drummond, E., Spriggs, H., Drummond, J., Magbanua, J.P., et al.; UK Drosophila Protein Trap Screening Consortium (2014). Analysis of the expression patterns, subcellular localisations and interaction partners of Drosophila proteins using a pigP protein trap library. Development *141*, 3994–4005.

Masuda, S., Oda, Y., Sasaki, H., Ikenouchi, J., Higashi, T., Akashi, M., Nishi, E., and Furuse, M. (2011). LSR defines cell corners for tricellular tight junction formation in epithelial cells. J. Cell Sci. *124*, 548–555.

Mechler, B.M., McGinnis, W., and Gehring, W.J. (1985). Molecular cloning of lethal(2)giant larvae, a recessive oncogene of Drosophila melanogaster. EMBO J. *4*, 1551–1557.

Nakai, K., Tanaka, T., Murai, T., Ohguro, N., Tano, Y., and Miyasaka, M. (2005). Invasive human pancreatic carcinoma cells adhere to endothelial tri-cellular corners and increase endothelial permeability. Cancer Sci. *96*, 766–773.

Noirot-Timothee, C., and Noirot, C. (1980). Septate and scalariform junctions in arthropods. Int. Rev. Cytol. *63*, 97–140.

Noirot-Timothée, C., Graf, F., and Noirot, C. (1982). The specialization of septate junctions in regions of tricellular junctions. II. Pleated septate junctions. J. Ultrastruct. Res. *78*, 152–165.

Oda, Y., Otani, T., Ikenouchi, J., and Furuse, M. (2014). Tricellulin regulates junctional tension of epithelial cells at tricellular contacts through Cdc42. J. Cell Sci. *127*, 4201–4212.

Oshima, K., and Fehon, R.G. (2011). Analysis of protein dynamics within the septate junction reveals a highly stable core protein complex that does not include the basolateral polarity protein Discs large. J. Cell Sci. *124*, 2861–2871.

Padash-Barmchi, M., Browne, K., Sturgeon, K., Jusiak, B., and Auld, V.J. (2010). Control of Gliotactin localization and levels by tyrosine phosphorylation and endocytosis is necessary for survival of polarized epithelia. J. Cell Sci. *123*, 4052–4062.

Padash-Barmchi, M., Charish, K., Que, J., and Auld, V.J. (2013). Gliotactin and Discs large are co-regulated to maintain epithelial integrity. J. Cell Sci. *126*, 1134–1143.

Paul, S.M., Ternet, M., Salvaterra, P.M., and Beitel, G.J. (2003). The Na+/K+ ATPase is required for septate junction function and epithelial tube-size control in the Drosophila tracheal system. Development *130*, 4963–4974.

Quiñones-Coello, A.T., Petrella, L.N., Ayers, K., Melillo, A., Mazzalupo, S., Hudson, A.M., Wang, S., Castiblanco, C., Buszczak, M., Hoskins, R.A., and Cooley, L. (2007). Exploring strategies for protein trapping in Drosophila. Genetics *175*, 1089–1104.

Riazuddin, S., Ahmed, Z.M., Fanning, A.S., Lagziel, A., Kitajiri, S., Ramzan, K., Khan, S.N., Chattaraj, P., Friedman, P.L., Anderson, J.M., et al. (2006). Tricellulin is a tight-junction protein necessary for hearing. Am. J. Hum. Genet. *79*, 1040–1051.

Richter, P.H., and Eigen, M. (1974). Diffusion controlled reaction rates in spheroidal geometry. Application to repressor—operator association and membrane bound enzymes. Biophys. Chem. *2*, 255–263.

Schulte, J., Tepass, U., and Auld, V.J. (2003). Gliotactin, a novel marker of tricellular junctions, is necessary for septate junction development in Drosophila. J. Cell Biol. *161*, 991–1000.

Schulte, J., Charish, K., Que, J., Ravn, S., MacKinnon, C., and Auld, V.J. (2006). Gliotactin and Discs large form a protein complex at the tricellular junction of polarized epithelial cells in Drosophila. J. Cell Sci. *119*, 4391–4401.

Schultz, J., Milpetz, F., Bork, P., and Ponting, C.P. (1998). SMART, a simple modular architecture research tool: identification of signaling domains. Proc. Natl. Acad. Sci. USA *95*, 5857–5864.

Snow, P.M., Bieber, A.J., and Goodman, C.S. (1989). Fasciclin III: a novel homophilic adhesion molecule in Drosophila. Cell *59*, 313–323.

Staehelin, L.A. (1973). Further observations on the fine structure of freeze-cleaved tight junctions. J. Cell Sci. *13*, 763–786.

Tepass, U., and Hartenstein, V. (1994). The development of cellular junctions in the Drosophila embryo. Dev. Biol. *161*, 563–596.

Tiklová, K., Senti, K.A., Wang, S., Gräslund, A., and Samakovlis, C. (2010). Epithelial septate junction assembly relies on melanotransferrin iron binding and endocytosis in Drosophila. Nat. Cell Biol. *12*, 1071–1077.

Whitlock, K.E. (1993). Development of Drosophila wing sensory neurons in mutants with missing or modified cell surface molecules. Development *117*, 1251–1260.

Woods, D.F., and Bryant, P.J. (1991). The discs-large tumor suppressor gene of Drosophila encodes a guanylate kinase homolog localized at septate junctions. Cell *66*, 451–464.

Wu, V.M., Schulte, J., Hirschi, A., Tepass, U., and Beitel, G.J. (2004). Sinuous is a Drosophila claudin required for septate junction organization and epithelial tube size control. J. Cell Biol. *164*, 313–323.